



CrossMark
click for updates

Cite this: *RSC Adv.*, 2014, 4, 37705

Immobilization of iron hydroxide/oxide on reduced graphene oxide: peroxidase-like activity and selective detection of sulfide ions†

Kuang-I Hsu,^a Chia-Wen Lien,^b Chia-Hua Lin,^c Huan-Tsung Chang^{*b}
and Chih-Ching Huang^{*ade}

We prepared nanocomposites of amorphous iron hydroxide/oxide immobilized on reduced graphene oxide (FeO_xH-rGO) with peroxidase-like activity for the detection of sulfide (S²⁻) ions. FeO_xH-rGO nanocomposites were prepared by reaction of GO (size ~ 300 nm) partially reduced by ultraviolet irradiation with Fe²⁺ in Tris-borate solution (5.0 mM, pH 7.0). The amorphous FeO(OH) and Fe(OH)₂ were immobilized on rGO to form FeO_xH-rGO nanocomposites. The as-prepared FeO_xH-rGO nanocomposites exhibited peroxidase-like catalytic activity in the H₂O₂-mediated oxidation of Amplex Red (AR) to fluorescent resorufin. Our AR/FeO_xH-rGO probe allowed the detection of H₂O₂ down to 50 nM within 10 min under microwave irradiation (170 W). The catalytic activity of FeO_xH-rGO was significantly suppressed in the presence of S²⁻ because of the formation of FeS on the FeO_xH-rGO nanocomposites' surfaces. The H₂O₂/AR-FeO_xH-rGO probe provided a limit of detection (signal-to-noise ratio = 3) of 50 nM for S²⁻ with high selectivity (>100-fold) with respect to other anions. Taking advantage of their high stability and selectivity, we employed our H₂O₂/AR-FeO_xH-rGO probe for the detection of S²⁻ in hot spring samples (75.1–619.5 μM) and the results showed good correlation (*r* = 0.98) with results from inductively coupled plasma mass spectrometry. This label-free, rapid, and simple sensing system shows great potential for the detection of S²⁻ ions in real samples.

Received 28th May 2014
Accepted 12th August 2014

DOI: 10.1039/c4ra05047a

www.rsc.org/advances

1 Introduction

Natural enzymes possess high substrate specificity and high catalytic efficiency, and have been extensively investigated in many applications such as medicine, environmental analysis, and food processing.¹ However, the catalytic activities of natural enzymes are easily affected by environmental conditions such as pH, temperature, ionic strength, surfactants, and organic solvents.² In recent years, great attention has been paid to the construction and discovery of novel enzyme mimetic

nanomaterials, specifically bimetallic nanoparticles (NPs) and hybrid nanomaterials.^{3–5} For example, it has been found that many noble metal-based NPs, including AuBi, AuPt, AuHg, AuPb, AgAu, and AgPt bimetallic alloy NPs, exhibit high catalytic activity.³ The enzyme-like activity (oxidase, peroxidase, and catalase) of Au NPs can be tuned by reaction of different metal ions.⁴ For example, Au NPs in the presence of Bi³⁺, Ag⁺, and Hg²⁺ exhibit peroxidase-, oxidase-, and catalase-like activities by forming AuBi, AuAg, and AuHg alloy nanolayers on particle surfaces, respectively.⁴ Furthermore, it has been demonstrated that graphene-based carbon materials promote electron transfer between the substrate and catalytic NPs, and improve their dispersibility.⁵ Many graphene-supported metal NPs or metal oxide NP hybrid nanomaterials, including Au@Pd nanoparticle-graphene hybrids, graphene oxide-Fe₃O₄ magnetic nanocomposites, Co₃O₄-reduced graphene oxide (rGO) nanocomposites, and CoFe₂O₄ immobilized on rGO nanocomposites, have been shown to act as peroxidase mimics for H₂O₂-mediated reactions.⁶ Furthermore, these graphene-based hybrid nanomaterials have been employed for the detection of glucose and DNA, and cancer cells and degradation of dyes.^{6,7}

The sulfide anion (S²⁻) is a traditional toxic pollutant found in water owing to not only industrial wastewater but also microbial reduction of sulfate by anaerobic bacteria and the sulfur-containing amino acids in meat proteins.⁸ Once

^aInstitute of Bioscience and Biotechnology, National Taiwan Ocean University, 2, Pei-Ning Road, Keelung, 20224, Taiwan. E-mail: huanging@ntou.edu.tw; Fax: +886-2-24622034; Tel: +886-2-24622192 ext. 5517

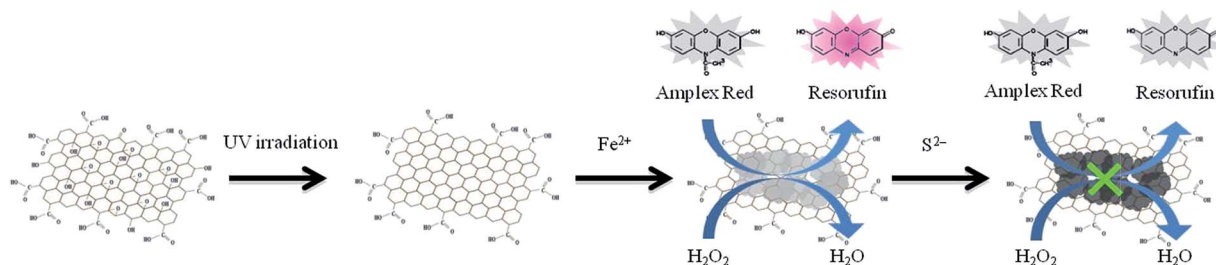
^bDepartment of Chemistry, National Taiwan University, 1, Section 4, Roosevelt Road, Taipei 10617, Taiwan. E-mail: changht@ntu.edu.tw; Fax: +886-2-33661171; Tel: +886-2-33661171

^cKey Laboratory for Nano-Bio Interface Research, Suzhou Key Laboratory for Nanotheranostics, Division of Nanobiomedicine, Suzhou Institute of Nano-Tech and Nano-Bionics, Chinese Academy of Sciences, Suzhou 215123, China

^dCenter of Excellence for Marine Bioenvironment and Biotechnology (CMBB), National Taiwan Ocean University, 2, Pei-Ning Road, Keelung, 20224, Taiwan

^eSchool of Pharmacy, College of Pharmacy, Kaohsiung Medical University, 100, Shih-Chuan 1st Road, Kaohsiung 80708, Taiwan

† Electronic supplementary information (ESI) available. Fig. S1–S9. See DOI: 10.1039/c4ra05047a



Scheme 1 Schematic representation of the preparation of peroxidase-like $\text{FeO}_x\text{H-rGO}$ nanocomposites for the detection of sulfide ions based on the inhibition of enzymatic activity.

protonated, H_2S is even more toxic than the sulfide itself. Continuous and high concentration exposure to H_2S can cause various physiological and biochemical problems such as Down's syndrome, Alzheimer's disease, diabetes, respiratory paralysis, and liver cirrhosis.⁹ Thus, a rapid and sensitive method for the detection of S^{2-} is essential for environmental protection, clinical diagnostics, and microbial infestations. So far, many methods have been employed for the determination of S^{2-} concentrations, including titration, spectroscopy, electrochemistry, chromatography, and combinations thereof.¹⁰ However, these probing systems are time-consuming, complicated procedures, requiring large sample volumes and specialized skills. Thus, there is a need to develop sensitive and simple probes not only for qualitative analysis but also for determination of S^{2-} in real samples at trace levels.

In this study, we immobilized iron hydroxide/oxide on rGO from rGO (size ~ 300 nm; prepared from irradiation of GO with UV light for 5 h) and iron ions (Fe^{2+}) in 5.0 mM Tris–borate solution (pH 7.0). The iron(III) oxide-hydroxide [$\text{FeO}(\text{OH})$] and iron(II) hydroxide [$\text{Fe}(\text{OH})_2$] were immobilized on rGO to form $\text{FeO}_x\text{H-rGO}$ nanocomposites. The $\text{FeO}_x\text{H-rGO}$ nanocomposites exhibited high catalytic activity for the H_2O_2 -mediated oxidation of Amplex Red (AR; 10-acetyl-3,7-dihydroxyphenoxazine) to fluorescent resorufin (7-hydroxy-3H-phenoxazin-3-one) (Scheme 1).¹¹ To demonstrate the practicality of $\text{FeO}_x\text{H-rGO}$, the as-prepared $\text{FeO}_x\text{H-rGO}$ nanocomposites were first employed for the rapid detection of H_2O_2 assisted with microwave irradiation. We further applied the $\text{AR}/\text{H}_2\text{O}_2$ - $\text{FeO}_x\text{H-rGO}$ system for the sensing of S^{2-} based on the analyte-induced inhibition of the catalytic activity of $\text{FeO}_x\text{H-rGO}$ nanocomposites (Scheme 1). The practicality of this approach was validated through the detection of S^{2-} in stream water, lake water, tap water, and hot springs.

2 Experimental

2.1 Chemicals

Tris(hydroxymethyl)aminomethane (Tris), hydrochloric acid, boric acid, and all metal salts used in this study were purchased from Mallinckrodt Baker (Phillipsburg, NJ, USA). AR was purchased from Invitrogen (Eugene, Oregon, USA). Sodium cyanide, sodium thiocyanate, sodium acetate, sodium bromide, sodium chloride, sodium carbonate, sodium iodide, sodium nitrate, sodium phosphate, potassium permanganate, sodium

sulfide, and graphite (7–11 μm) were obtained from Alfa Aesar (Ward Hill, MA, USA). Hydrogen peroxide was purchased from SHOWA (Tokyo, Japan). Sulfuric acid and phosphoric acid were purchased from J. T. Baker (Phillipsburg, NJ, USA). Milli-Q ultrapure water (Millipore, Billerica, MA, USA) was used in all experiments. The buffer used in this study was a solution of Tris–borate (50 mM, pH 7.0 adjusted Tris with 200 mM boric acid).

2.2 Preparation of $\text{FeO}_x\text{H-rGO}$

GO was synthesized using an improved Hummers' method.¹² Briefly, a mixture of graphite flakes (0.75 g) and KMnO_4 (4.5 g) was added to a 9 : 1 mixture of concentrated H_2SO_4 and H_3PO_4 (100 mL). The mixture was then heated to 50 $^\circ\text{C}$ and stirred for 12 h. The reaction was cooled to room temperature in an ice bath, and then poured into 100 mL of deionized (DI) water containing 3 mL of 30% H_2O_2 . The aqueous mixture was then centrifuged at a relative centrifugal force of 35 000g for 1 h, and the supernatant was decanted. The remaining pellet was repeatedly washed with 200 mL of DI water until the washings reached a pH of 7.0. The aqueous solution was then sonicated for 1 h and centrifuged at a relative centrifugal force of 25 000g for 0.5 h. The GO solution was collected and the remaining pellet was discarded. The GO concentration in the supernatant was determined to be ~ 1.2 g L^{-1} (denoted as the 100 \times concentration for simplicity) using the freeze-drying method. The reduced graphene oxide (rGO) was prepared from irradiation of 10 \times GO in 5.0 mM Tris–borate solution (pH 7.0) with a hand-held UV lamp (365 nm; 140 mW cm^{-2}) for 5 h. For preparation of $\text{FeO}_x\text{H-rGO}$, FeCl_2 (100 μM) was mixed with GO (1 \times) in a Tris–borate solution (5.0 mM, pH 7.0) and reacted for 1 h. The resulting $\text{FeO}(\text{OH})$ and $\text{Fe}(\text{OH})_2$ were immobilized on rGO to form the $\text{FeO}_x\text{H-rGO}$ nanocomposites.

2.3 Characterization

Transmission electron microscope (TEM) images of the rGO and $\text{FeO}_x\text{H-rGO}$ nanocomposites were recorded using a Hitachi H7100 TEM, operated at 75 kV. Samples for TEM and energy-dispersive X-ray spectroscopy (EDS) measurements were prepared by placing aliquots (20 μL) of the rGO or $\text{FeO}_x\text{H-rGO}$ solutions on a carbon-coated copper grid (copper 200 mesh). After standing for 2 h at ambient temperature, the solution of rGO or $\text{FeO}_x\text{H-rGO}$ was removed. EDS analysis of $\text{FeO}_x\text{H-rGO}$

using a 0.7 nm diameter electron probe was employed to determine their chemical identities. X-ray diffraction (XRD) samples were prepared by depositing FeO_xH-rGO on a Si(100) wafer, and XRD measurements were performed at room temperature using a Rigaku 18 kW rotating anode source X-ray diffractometer (The Woodlands, Texas, USA) with the Cu K α 1 line ($\lambda = 1.54 \text{ \AA}$, energy = 8.8 keV) operated at 50 kV, 100 mA, and slits set at $10 \times 2 \text{ mm}^2$. X-ray photoelectron spectroscopy (XPS) was performed using a VG ESCA scientific theta probe spectrometer (Uppsala, Sweden) in the constant analyzer energy mode with a pass energy of 28 eV and Al K α (1486.6 eV) radiation as the excitation source. Raman spectra were recorded using a Raman spectrometer (DongWoo 500i; KyungGiDo, Korea) equipped with a 50 \times objective Nd:YAG laser (532 nm) and a charge-coupled detector. The signal collection time for each sample was 30 s. A Zetasizer 3000HS analyzer (Malvern Instruments, Malvern, UK) was used for analysis of dynamic light scattering and zeta potential of rGO and FeO_xH-rGO nanocomposites.

2.4 Peroxidase-like activity assay

Aliquots (400 μL) of Tris-borate solutions (5.0 mM, pH 7.0) containing Fe²⁺ (125 μM), GO (1.25 \times), FeO_xH-GO (1.25 \times), rGO (1.25 \times), or FeO_xH-rGO (1.25 \times) were equilibrated at room temperature for 1 h. Tris-borate solution (100 μL , 5.0 mM, pH 7.0) containing AR (50 μM) and H₂O₂ (500 μM) was then added to each of the mixtures and left for 2 h before fluorescence measurements with excitation at 530 nm (Synergy 4 monochromatic microplate spectrophotometer, Biotek Instruments, Winooski, VT, USA).

2.5 Catalytic sensing of S²⁻

Aliquots (350 μL) of the Tris-borate solution (5.0 mM, pH 7.0) containing FeO_xH-rGO (0.143 \times) were equilibrated at room temperature for 10 min. Tris-borate solution (50 μL , 5.0 mM, pH 7.0) containing S²⁻ (0–15 μM) was separately added to each of the FeO_xH-rGO nanocomposite solutions and left for an additional 30 min. Tris-borate solution (100 μL , 5.0 mM, pH 7.0) containing AR (50 μM) and H₂O₂ (50 μM) was then added to each of the mixtures and left for 2 h before fluorescence measurements with excitation at 530 nm.

2.6 Enzyme kinetic analysis

Kinetic measurements were conducted with a black 96-well microplate using a Synergy 4 monochromatic microplate spectrophotometer. The AR/H₂O₂ substrates in Tris-borate solution (180 μL , pH 7.0) were separately added to each well of a microtiter plate, and aliquots (20 μL) of peroxidase-like FeO_xH-rGO nanocomposite solutions (1 \times) were then added to the plate. The reaction progress was monitored every 30 s for 2 h by recording the fluorescence of the reaction product, resorufin, at 585 nm with an excitation wavelength of 530 nm. Variable concentrations (0.5–25 μM) of AR with a constant H₂O₂ concentration (10 μM) were investigated in the catalytic reactions. In addition, variable H₂O₂ concentrations (100–7500 μM)

with a constant AR concentration (10 μM) were also investigated.

2.7 Analysis of real samples

Water samples collected from a stream near the National Taiwan Ocean University campus, a lake on the National Taiwan University campus, and local tap water were filtered through a 0.22 μm membrane. For the detection of S²⁻, aliquots (300 μL) of the Tris-borate solution (5.0 mM, pH 7.0) containing FeO_xH-rGO (0.167 \times) were equilibrated at room temperature for 10 min. The 2-fold diluted water samples were spiked with S²⁻ (0–5.0 μM) in a Tris-borate solution (100 μL , 5.0 mM, pH 7.0) and then separately added to the FeO_xH-rGO nanocomposite solutions. After reacting for 30 min, the Tris-borate solution (100 μL , 5.0 mM, pH 7.0) containing AR (50 μM) and H₂O₂ (50 μM) was added to each of the mixtures and left for 2 h before fluorescence measurements with excitation at 530 nm.

Hot spring water samples collected from Yangmingshan National Park were filtered through a 0.22 μm membrane. For the detection of S²⁻, aliquots (300 μL) of the Tris-borate solution (5.0 mM, pH 7.0) containing FeO_xH-rGO (0.167 \times) were equilibrated at room temperature for 10 min. The 40-fold diluted hot spring water samples were prepared in a Tris-borate solution (100 μL , 5.0 mM, pH 7.0) and then separately added to the FeO_xH-rGO nanocomposite solutions. After reacting for 30 min, the Tris-borate solution (100 μL , 5.0 mM, pH 7.0) containing AR (50 μM) and H₂O₂ (50 μM) was added to each of the mixtures and left for 2 h before fluorescence measurements with excitation at 530 nm. Moreover, all samples were analyzed by inductively coupled plasma-mass spectrometry (ICP-MS; 7700 Series, Agilent Technologies, California, USA); the samples were prepared in 2% HNO₃.

3 Results and discussion

3.1 Peroxidase-like activity of FeO_xH-rGO

The peroxidase-like activity of the FeO_xH-rGO nanocomposites was evaluated using the typical peroxidase substrate AR in the presence of H₂O₂. H₂O₂ acted as an electron acceptor of the FeO_xH-rGO nanocomposites for the catalytic oxidation of AR with a 1 : 1 stoichiometry, which yielded a highly fluorescent and colored product, resorufin (quantum yield: 0.83; absorption coefficient: $5.4 \times 10^4 \text{ cm}^{-1} \text{ M}^{-1}$ at 570 nm).¹³ The AR was selected as the substrate based on the stability of its oxidized product (resorufin) at pH values greater than 5.0 and its high quantum yield (>80%) as well as long excitation and emission wavelengths. Moreover, fluorescence-based sensors are typically much sensitive (>100-fold) than colorimetric ones, we expected our H₂O₂/AR-FeO_xH-rGO probe to provide a comparatively lower LOD values for S²⁻. In our previous study,¹⁴ we found that 3,3',5,5'-tetramethylbenzidine (TMB) was not a suitable substrate for nanoparticles-mediated catalytic oxidation of AR in the presence of H₂O₂ in neutral solution, mainly because TMB could only react with H₂O₂ by natural peroxidase and peroxidase mimic nanoparticles at low pH values (3.0–5.0). The FeO_xH-rGO nanocomposites likely catalyzed a one-electron

oxidation of a nonfluorescent AR to form a nonfluorescent AR radical.¹⁵ Subsequently, these two AR radicals underwent an enzyme-independent dismutation reaction to form fluorescent resorufin. The Fe^{2+} , GO, and rGO exhibited relatively low catalytic activity for the H_2O_2 -mediated AR reaction (curves a, b, and d in Fig. 1A). In contrast, the FeO_xH -GO and FeO_xH -rGO (curves c and e in Fig. 1A) relative to GO and rGO exhibited 70- and 770-fold fluorescence intensity at 585 nm when excited at 530 nm. Our results indicated that FeO_xH -rGO nanocomposites have high peroxidase-like activity. The catalytic mechanism of FeO_xH -rGO nanocomposites may follow Fenton-like reactions due to $\text{Fe}^{2+}/\text{Fe}^{3+}$ in deposited FeO_xH .¹⁶ When FeCl_2 was prepared in Tris–borate solution (5.0 mM, pH 7.0), the iron(III) oxide-hydroxide ($4\text{Fe}^{2+} + \text{O}_2 + 6\text{H}_2\text{O} \rightarrow 4\text{FeO}(\text{OH}) + 8\text{H}^+$) and iron(II) hydroxide ($\text{Fe}^{2+} + 2\text{H}_2\text{O} \rightarrow \text{Fe}(\text{OH})_2 + 2\text{H}^+$) were formed and immobilized on GO or rGO.¹⁶ As shown in Fig. 2B and C, the FeO_xH nanostructures were randomly distributed on the surface of GO and rGO.

The Raman spectra of FeO_xH -rGO revealed that the $\text{FeO}(\text{OH})$ and $\text{Fe}(\text{OH})_2$ species were dominant on rGO (Fig. S1, ESI†). The peaks at 210, 272, 384, and 995 cm^{-1} were assigned to $\text{FeO}(\text{OH})$, while the bands at 580 cm^{-1} were attributed to $\text{Fe}(\text{OH})_2$. In addition, the atomic ratio of O to Fe of bare FeO_xH was evaluated by the EDS measurement to be about 1.98 : 1, consistent with that of FeOOH or $\text{Fe}(\text{OH})_2$ (Fig. S2, ESI†). The XPS

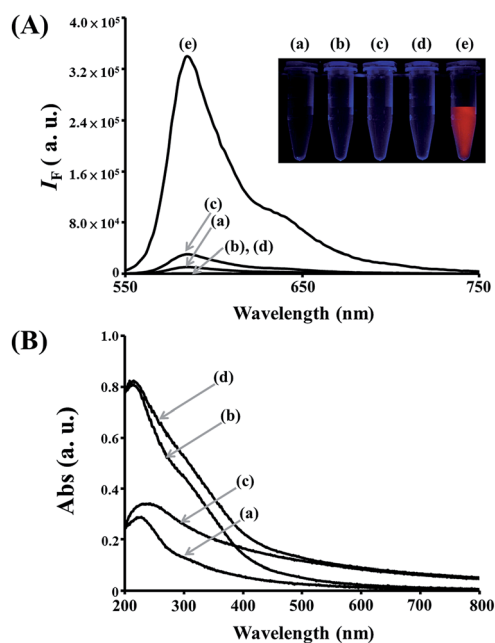


Fig. 1 (A) Fluorescence spectra of 5.0 mM Tris–borate (pH 7.0) containing AR (10 μM) and H_2O_2 (100 μM) in the presence of (a) Fe^{2+} (100 μM), (b) GO (1 \times), (c) FeO_xH -GO [prepared from GO (1 \times) and Fe^{2+} (100 μM) in Tris–borate solution], (d) rGO (1 \times), and (e) FeO_xH -rGO [prepared from rGO (1 \times) and Fe^{2+} (100 μM) in Tris–borate solution]. (B) UV-vis absorption spectra of 5.0 mM Tris–borate (pH 7.0) in the presence of (a) GO, (b) FeO_xH -GO, (c) rGO, and (d) FeO_xH -rGO. Inset to (A): photograph of the fluorescence of the solutions upon excitation under a hand-held UV lamp (365 nm). The fluorescence intensity (I_F) and absorption (Abs) are plotted in arbitrary units (a. u.). The excitation wavelength in (A) was set at 530 nm.

measurement further revealed the $\text{FeO}(\text{OH})$ (43.2%) and $\text{Fe}(\text{OH})_2$ (50.4%) are the major species in the FeO_xH -rGO nanocomposite (Fig. S3, ESI†). Moreover, no crystalline FeO_xH was found in the XRD image (data not shown), suggesting that the deposited $\text{FeO}(\text{OH})$ and $\text{Fe}(\text{OH})_2$ are amorphous. Recently, amorphous FeOOH and $\text{Fe}(\text{OH})_2$ nanostructures have been employed as catalysts for photoelectrochemical water splitting, electrode materials for lithium-ion batteries, and degradation of dye pollutants.^{17,18} To our knowledge, however, amorphous FeOOH and $\text{Fe}(\text{OH})_2$ used as enzyme-like materials in solution have not been attempted, although its specific surface area is higher than crystalline iron oxide (such as Fe_2O_3 and Fe_3O_4). FeOOH and $\text{Fe}(\text{OH})_2$ are merely used as catalysts in homogeneous aqueous solution, probably because their nanostructures are difficult to confine; they easily exist as gel-like structures suspended in the solution. Another disadvantage of amorphous FeOOH and $\text{Fe}(\text{OH})_2$ is their tendency to form crystalline iron oxides or dissolve in preparation or storage, which may greatly reduce their catalytic activity as their surface area is greatly diminished. We noted that our rGO-supported $\text{FeO}(\text{OH})$ and $\text{Fe}(\text{OH})_2$ were stable in aqueous solution at room temperature for at least two months. This phenomenon is presumably due to the strong association of $\text{FeO}(\text{OH})$ and $\text{Fe}(\text{OH})_2$ with rGO, improving their stability.

We noted that the peroxidase-like activity of FeO_xH -rGO (curve e in Fig. 1) was about 10-fold higher than that of FeO_xH -GO (curve c in Fig. 1). This may be attributed to the fact that rGO has a stronger adsorption ability to AR and higher conductivity.¹⁹ The UV-vis absorption spectra of GO show a broad absorption band with a shoulder in the UV region. The absorption band (230 nm) was attributed to the $\pi \rightarrow \pi^*$ transition of the $\text{C}=\text{C}$ bond in the sp^2 hybrid region. The shoulder at $\sim 300\text{ nm}$ was caused by the $n \rightarrow \pi^*$ electronic transition of peroxide and/or epoxide functional groups in GO.²⁰ The slightly stronger absorption of rGO indicated that some oxygen-containing carbons were reduced to $\text{C}=\text{C}$, which can provide more π orbitals for adsorption of AR molecules *via* π - π stacking and transfer of electrons to oxidize AR. Relative to GO, the higher ratio of $\text{C}=\text{C}/\text{C}-\text{C}$ (86.2% *versus* 56.9%; Fig. S4, ESI†) of rGO further supports our reasoning. We also noted that at constant concentrations of AR (500 nM) and GO or rGO (1 \times), about 70% and 95% of AR molecules were adsorbed on GO and rGO, respectively. It has been reported that enzyme-mimicking nanoparticles transfer electrons between pairs of different oxidation states of metal ions to drive their catalytic activity.^{3–5} Therefore, the various valence states of $\text{Fe}^{2+}/\text{Fe}^{3+}$ on particle surfaces and high conductivity of rGO accounted for the nanocomposites' high peroxidase-like activity.

3.2 Effect of irradiation

We demonstrated that rGO plays an important role in enhancing the catalytic activity of FeO_xH . Fig. 3 shows that the catalytic activity of FeO_xH -rGO nanocomposites was increased with increasing UV-irradiation time in the preparation of rGO. The fluorescence intensity of resorufin at 585 nm increased initially on increasing the irradiation time before reaching a

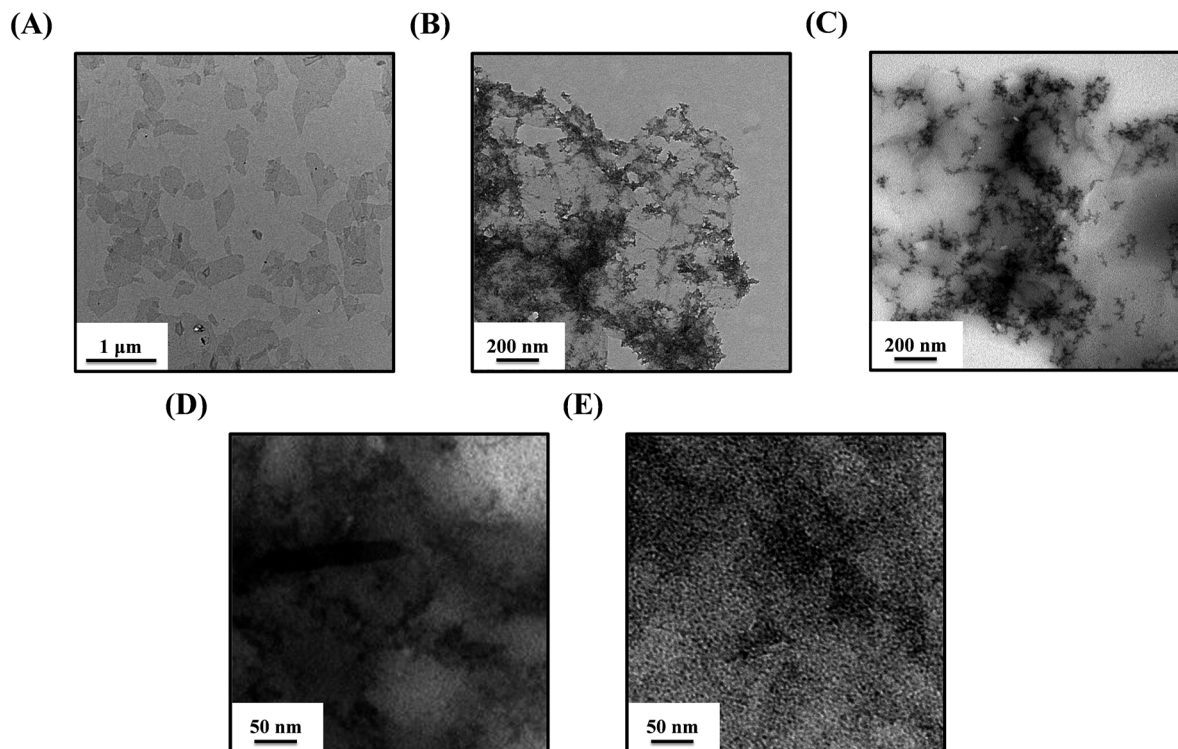


Fig. 2 (A–C) Low-magnification TEM images of 5.0 mM Tris–borate (pH 7.0) containing (A) rGO (1 \times), (B) FeO_xH–GO (1 \times), and (C) FeO_xH–rGO (1 \times) and (D and E) high-magnification TEM images of 5.0 mM Tris–borate (pH 7.0) containing (D) FeO_xH–GO (1 \times) and (E) FeO_xH–rGO (1 \times). Other conditions were the same as those described in Fig. 1.

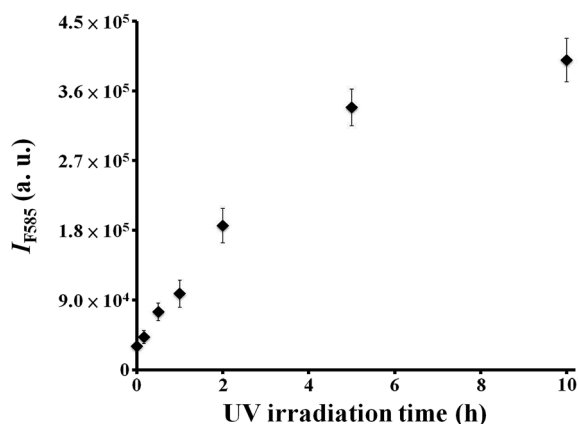


Fig. 3 Fluorescence response (I_{F585}) of 5.0 mM Tris–borate (pH 7.0) containing AR (10 μ M), H₂O₂ (100 μ M), and FeO_xH–rGO [prepared from Fe²⁺ (100 μ M) and UV-irradiated (0–10 h) GO (1 \times)]. Error bars represent the standard deviations from three repeated experiments. The fluorescence intensities at 585 (I_{F585}) are plotted in arbitrary units (a. u.). Other conditions were the same as those described in Fig. 1.

plateau at \sim 5 h. This result is consistent with the UV-vis absorption of rGO, which was prepared from GO with different UV-irradiation times (0–10 h; Fig. S5, ESI[†]). The color of GO (rGO) solutions changed from light brown to dark black and absorbance became stronger with increasing UV-irradiation time, from 0 to 10 h. Under optimized conditions for the preparation of rGO (irradiation of GO with UV light for 5 h), our

AR–FeO_xH–rGO probe allowed detection of H₂O₂ concentrations down to 1.0 μ M under the catalytic reaction time of 2 h (curve a in Fig. S6, ESI[†]). To shorten the analysis time (<10 min), we employed microwave irradiation to aid the catalytic reaction. Microwave heating is one type of electroheating technique that utilizes specific wavelengths of electromagnetic energy.²¹ When applying microwave irradiation to metallic and metal oxide nanomaterials, the electric and magnetic components change rapidly, and the molecules cannot respond quickly to the change in direction, giving rise to friction and therefore causing them to quickly warm up.²² The acceleration of the catalytic reaction rate of H₂O₂/AR–FeO_xH–rGO under microwave irradiation is probably due to the superheating effect produced in a microwave field.²³ The heat and electron transfer of FeO_xH–rGO was strongly influenced after GO interacted with the microwave field.²⁴ It has been demonstrated that metal oxide–rGO nanocomposites have better dielectric constants due to the significantly increased conductivity from rGO.²⁴ Metal oxides incorporated with rGO could have enhanced microwave-absorbing properties.²⁵ In addition, the different dielectric properties of the liquid and FeO_xH–rGO nanocomposites might result in localized temperature differences, creating strong convection currents at the surface of the microwaved FeO_xH–rGO nanocomposites.^{24,25} Therefore, diffusions of the reaction products were rapidly promoted away from the surface. Under the assistance of microwave irradiation (170 W), our AR–FeO_xH–rGO probe allowed the detection of H₂O₂ with a limit of detection (LOD; signal-to-noise (S/N) ratio = 3) of

~50 nM within 10 min (curve b in Fig. S5, ESI†). One of the possible factors for this ultrahigh sensitivity for H₂O₂ is the microwave temperature; under microwave irradiation of 170 W, the reaction temperature was raised to ~75 °C. However, we noted that the reaction time needed to reach completion was 2 h even at 75 °C (data not shown). In another control experiment, we noted the microwave irradiation caused negligible fluorescence change to 5.0 mM Tris–borate (pH 7.0) solution containing AR (10 μM)–H₂O₂ (10 μM). This microwave-assisted catalytic reaction not only shortened the analysis time to 10 min, but also provided near one order of magnitude greater sensitivity than the above results. Compared with other GO-based nanocomposites with peroxidase-like activities, the preparation of FeO_xH–rGO is relatively simple and cost-effective and the AR–FeO_xH–rGO probe shows comparable sensitivity for H₂O₂ detection.^{6,7}

3.3 Sensing of sulfide

Fig. 4A (curve b) reveals the poorly developed fluorescence intensity of the H₂O₂/AR–FeO_xH–rGO (0.1×) system in the presence of S²⁻ (10 μM) in Tris–borate solution (5.0 mM, pH 7.0). The low catalytic activity of FeO_xH–rGO in the presence of S²⁻ is presumably because of the formation of FeS and Fe₂S₃ on the FeO_xH–rGO due to the strong affinity of S²⁻ for surface iron ions on nanocomposites Fe²⁺ ($K_{sp}(\text{FeS}) \sim 6 \times 10^{-19}$) and Fe³⁺ ($K_{sp}(\text{Fe}_2\text{S}_3) \sim 1 \times 10^{-88}$). The formation of FeS and Fe₂S₃ may block the active sites of FeO_xH–rGO and diminish their peroxidase-like activity. The EDS (Fig. 4B) and Raman spectra (Fig. 4C) further supported that sulfide was deposited on FeO_xH–rGO. In addition, we used ICP-MS to quantify that about 95% of S²⁻ (10 μM) ions were binding to FeO_xH–rGO (0.1×). According to the Michaelis–Menten

Table 1 Comparison of the apparent Michaelis constant (K_M) and maximal velocity (v_{max}) between FeO_xH–rGO nanocomposites (0.1×) in the absence and presence of S²⁻ (10 μM)

Catalyst	Substrate	K_M (μM)	v_{max} (μM s ⁻¹)
FeO _x H–rGO	AR	3.67	1.3×10^{-3}
FeO _x H–rGO + S ²⁻	AR	5.16	7.1×10^{-4}
FeO _x H–rGO	H ₂ O ₂	326	5.6×10^{-4}
FeO _x H–rGO + S ²⁻	H ₂ O ₂	166	2.2×10^{-4}

equation ($1/\nu = K_M/\nu_{max} (1/[S] + 1/K_M)$), the kinetic data, including the Michaelis constant (K_M) and maximal velocity (ν_{max}) of FeO_xH–rGO nanocomposites in the absence and presence of S²⁻, were calculated and are listed in Table 1. From the double reciprocal plots of catalytic velocity against one of the substrate concentrations when the other substrate was fixed at three concentration levels, we demonstrated that the catalytic reaction of H₂O₂/AR–FeO_xH–rGO followed a ping-pong mechanism because the slopes of the lines were parallel (Fig. S7, ESI†).²⁶ This result revealed that, like HRP, the FeO_xH–rGO nanocomposites bind and react with the first substrate (AR or H₂O₂) and then release the first product before reacting with the other substrate. K_M is often associated with the affinity of the catalyst NPs for the substrates. By comparing the apparent kinetic parameters, the K_M value of FeO_xH–rGO nanocomposites in the presence of S²⁻ with AR as the substrate was slightly higher than that in the absence of S²⁻, revealing that FeO_xH–rGO nanocomposites have a lower affinity with AR when FeS and/or Fe₂S₃ were deposited on their surfaces. The K_M value of FeO_xH–rGO nanocomposites in the presence of S²⁻ with H₂O₂ as the substrate was slightly lower than that for FeO_xH–rGO nanocomposites alone, which agrees with reports that FeS and Fe₂S₃ have a strong affinity with H₂O₂.²⁷ Although FeO_xH–rGO nanocomposites in the presence of S²⁻ have a lower K_M for H₂O₂, the ~2.5-fold lower ν_{max} value indicated that the deposited FeS and Fe₂S₃ did not promote the catalytic reaction.

We further investigated the selectivity and sensitivity of the H₂O₂ (10 μM)/AR (10 μM)–FeO_xH–rGO (0.1×) probe for sensing S²⁻. The catalytic activity of FeO_xH–rGO was significantly reduced by S²⁻ at room temperature, when compared with other tested anions, including CH₃COO⁻, PO₄³⁻, S₂O₃²⁻, SO₄²⁻, NO₃⁻, Cl⁻, Br⁻, I⁻, NO₂⁻, CN⁻, SCN⁻, AsO₂⁻, and AsO₄³⁻ (Fig. 5A, the concentration of each anion was 10 μM). In addition, tolerance concentrations of the other anions (within a relative error of ±5%) during the sensing of S²⁻ (10 μM) with the H₂O₂/AR–FeO_xH–rGO probe were at least 100 times higher than that of the S²⁻ (Fig. S8, ESI†). The fluorescence response of the H₂O₂/AR–FeO_xH–rGO probe decreased on increasing the concentration of S²⁻ ions (Fig. 5B). We obtained a linear response in the plot of the expression $(I_{F0} - I_F)/I_{F0}$ against the concentration of S²⁻ over the range 0.1–1.5 μM ($r = 0.99$), where I_{F0} and I_F represent the fluorescence intensities of the mixtures in the absence and presence, respectively, of the added S²⁻. The H₂O₂/AR–FeO_xH–rGO probe provided an LOD for S²⁻ ions ($S/N = 3$) of ~50 nM. This LOD for S²⁻ was comparable to those using other optical sensors with functional nanoparticles.^{28,29}

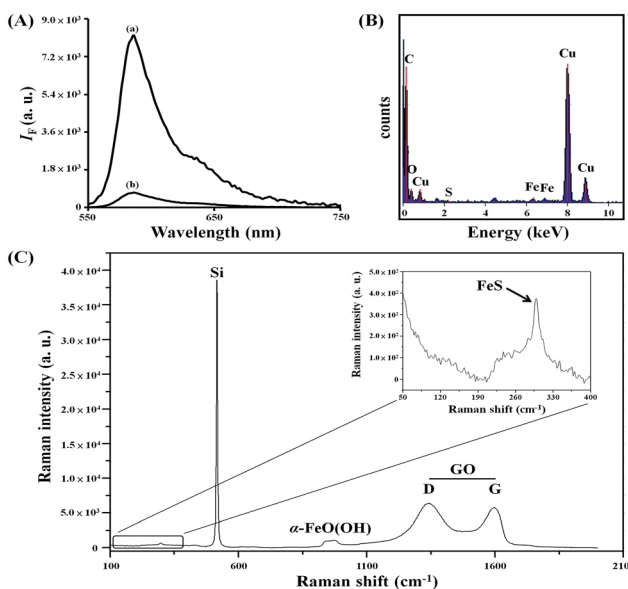


Fig. 4 (A) Fluorescence spectra of 5.0 mM Tris–borate (pH 7.0) containing AR (10 μM), H₂O₂ (10 μM), and FeO_xH–rGO (0.1X) in the (a) absence and (b) presence of S²⁻ (10 μM). (B) EDS and (C) Raman spectra of FeO_xH–rGO (10X) in the presence of S²⁻ (1.0 mM).

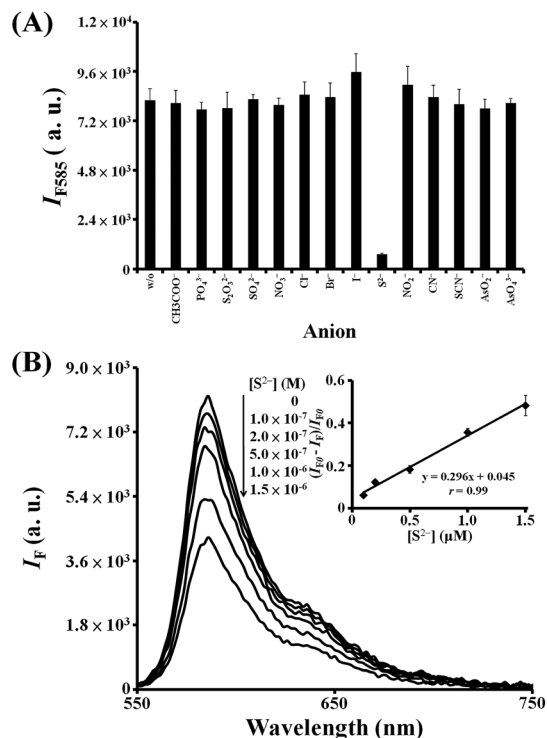


Fig. 5 (A) Selectivity of the $\text{H}_2\text{O}_2/\text{AR}-\text{FeO}_x\text{H}-\text{rGO}$ probe toward S^{2-} ions. Fluorescence response (I_{F585}) of 5.0 mM Tris–borate solution (pH 7.0) containing AR (10 μM), H_2O_2 (10 μM), and $\text{FeO}_x\text{H}-\text{rGO}$ nanocomposites (0.1 \times) in the absence or presence of anions (10 μM) at 585 nm. (B) Validation of the use of $\text{H}_2\text{O}_2/\text{AR}-\text{FeO}_x\text{H}-\text{rGO}$ probe for the detection of S^{2-} (0–1.5 μM). The inset to (B): values of $(I_{F0} - I_F)/I_{F0}$ were plotted against S^{2-} concentration. I_{F0} and I_F represent the fluorescence intensities of the solutions at 585 nm in the absence and presence of S^{2-} , respectively. Error bars in the inset represent the standard deviations from three repeated experiments. Other conditions were the same as those described in Fig. 4.

Although the sensitivities of some chemosensors are higher than the $\text{H}_2\text{O}_2/\text{AR}-\text{FeO}_x\text{H}-\text{rGO}$ probe, those chemosensors require complicated and multistep complicated synthesis and use of sophisticated equipment.³⁰

3.4 Detection of S^{2-} in real samples

To validate that our proposed sensing strategy could have practical application for S^{2-} analysis in water samples, we applied the $\text{H}_2\text{O}_2/\text{AR}-\text{FeO}_x\text{H}-\text{rGO}$ sensor to determine the levels of S^{2-} in stream, lake, and tap water samples. Before analysis, each of the three samples were filtered through a 0.22 μm membrane and diluted 10-fold in 5.0 mM Tris–borate solution (pH 7.0). Here, we obtained linear correlations ($r = 0.98\text{--}0.99$) between the relative fluorescence changes $((I_{F0} - I_F)/I_{F0})$ and the concentration of spiked S^{2-} (Fig. S9, ESI[†]), where I_{F0} and I_F represent the fluorescence intensities of the mixtures in the absence and presence, respectively, of the spiked S^{2-} . In these measurements, the probe provided recoveries of 104.2–107.3% for S^{2-} ions (0.5 μM). The minimum concentration of S^{2-} ions detectable by our $\text{H}_2\text{O}_2/\text{AR}-\text{FeO}_x\text{H}-\text{rGO}$ probe in these water samples was ~ 100 nM. Neither an ICP-MS-based system nor our

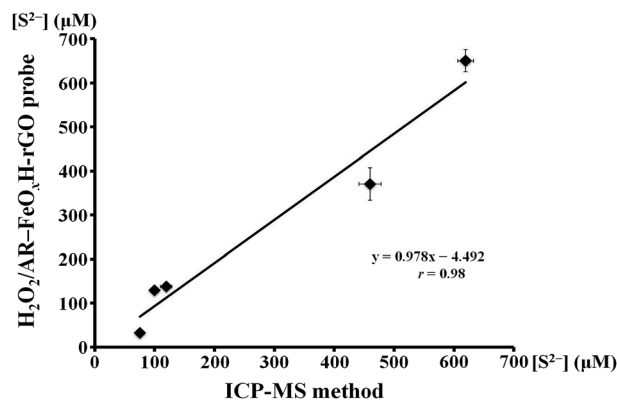


Fig. 6 Comparison between ICP-MS and the $\text{H}_2\text{O}_2/\text{AR}-\text{FeO}_x\text{H}-\text{rGO}$ probe for detection of S^{2-} in hot spring water samples. There was a linear correlation between the S^{2-} concentrations in five hot spring waters determined using ICP-MS and $\text{H}_2\text{O}_2/\text{AR}-\text{FeO}_x\text{H}-\text{rGO}$ assays. Error bars represent the standard deviations from three repeated experiments.

sensing approach could detect the presence of any S^{2-} ions in these original water samples. We further applied the $\text{H}_2\text{O}_2/\text{AR}-\text{FeO}_x\text{H}-\text{rGO}$ probe to determine the S^{2-} ions in five sulfur spring waters collected from Yangmingshan National Park (Taipei, Taiwan). Fig. 6 shows the good linear correlation ($r = 0.98$) between the results obtained using the $\text{H}_2\text{O}_2/\text{AR}-\text{FeO}_x\text{H}-\text{rGO}$ probe and ICP-MS over concentrations ranging from 75.1 to 619.5 μM , suggesting that our probe is useful for screening S^{2-} concentrations in hot spring waters. Therefore, the proposed methods are applicable for practical analysis of S^{2-} in environmental samples.

4 Conclusions

In summary, nanocomposites of amorphous FeO_xH immobilized on rGO ($\text{FeO}_x\text{H}-\text{rGO}$) were successfully synthesized by the simple reaction of GO partially reduced by ultraviolet irradiation with Fe^{2+} in aqueous solution. We demonstrated that $\text{FeO}_x\text{H}-\text{rGO}$ nanocomposites exhibit intrinsic peroxidase-like activity. With the assistance of microwave irradiation, our $\text{AR}/\text{FeO}_x\text{H}-\text{rGO}$ probe allowed detection of H_2O_2 down to 50 nM within 10 min. In the presence of S^{2-} , the catalytic activity of $\text{FeO}_x\text{H}-\text{rGO}$ became lower because the formation of FeS and Fe_2S_3 may block the active sites of $\text{FeO}_x\text{H}-\text{rGO}$. The $\text{H}_2\text{O}_2/\text{AR}-\text{FeO}_x\text{H}-\text{rGO}$ probe provided an LOD of 50 nM for S^{2-} with high selectivity (>100 -fold). Owing to the high stability and selectivity of the nanocomposites, the $\text{H}_2\text{O}_2/\text{AR}-\text{FeO}_x\text{H}-\text{rGO}$ probe allowed the detection of S^{2-} in hot spring waters (75.1–619.5 μM) and the results showed good correlation ($r = 0.98$) with ICP-MS. This label-free, low cost, and rapid nanosensor holds great potential for screening S^{2-} in real water samples.

Acknowledgements

This study was supported by the Ministry of Science and Technology of Taiwan under contracts NSC 101-2628-M-019-

001-MY3, 102-2113-M-019-001-MY3 and 102-2627-M-019-001-MY3.

Notes and references

- (a) L. M. Podust and D. H. Sherman, *Nat. Prod. Rep.*, 2012, **29**, 1251–1266; (b) J. A. Gerlt and P. C. Babbitt, *Curr. Opin. Chem. Biol.*, 2009, **13**, 10–18; (c) R. Masella, R. Di Benedetto, R. Vari, C. Filesi and C. Giovannini, *J. Nutr. Biochem.*, 2005, **16**, 577–586.
- (a) M. Naushad, Z. A. ALOthman, A. B. Khan and M. Ali, *Int. J. Biol. Macromol.*, 2012, **51**, 555–560; (b) P. V. Iyer and L. Ananthanarayan, *Process Biochem.*, 2008, **43**, 1019–1032; (c) C. Mateo, J. M. Palomo, G. Fernandez-Lorente, J. M. Guisan and R. Fernandez-Lafuente, *Enzyme Microb. Technol.*, 2007, **40**, 1451–1463; (d) G. Feller, *J. Phys.: Condens. Matter*, 2010, **22**, 323101; (e) S. Yabuki, *Anal. Sci.*, 2014, **30**, 213–217.
- (a) C.-W. Lien, C.-C. Huang and H.-T. Chang, *Chem. Commun.*, 2012, **48**, 7952–7954; (b) W. He, Y. Liu, J. Yuan, J.-J. Yin, X. Wu, X. Hu, K. Zhang, J. Liu, C. Chen, Y. Ji and Y. Guo, *Biomaterials*, 2011, **32**, 1139–1147; (c) C.-I. Wang, C.-C. Huang, Y.-W. Lin, W.-T. Chen and H.-T. Chang, *Anal. Chim. Acta*, 2012, **745**, 124–130; (d) C.-I. Wang, W.-T. Chen and H.-T. Chang, *Anal. Chem.*, 2012, **84**, 9706–9712; (e) H. You, Z. Peng, J. Wu and H. Yang, *Chem. Commun.*, 2011, **47**, 12595–12597; (f) Y. Chen, H. Cao, W. Shi, H. Liu and Y. Huang, *Chem. Commun.*, 2013, **49**, 5013–5015.
- C.-W. Lien, Y.-C. Chen, H.-T. Chang and C.-C. Huang, *Nanoscale*, 2013, **5**, 8227–8234.
- (a) J. Zhu, M. Chen, Q. He, L. Shao, S. Wei and Z. Guo, *RSC Adv.*, 2013, **3**, 22790–22824; (b) B. F. MacHado and P. Serp, *Catal. Sci. Technol.*, 2012, **2**, 54–75; (c) G. Blanita and M. D. Lazar, *Micro Nanosyst.*, 2013, **5**, 138–146; (d) Y. Liang, Y. Li, H. Wang and H. Dai, *J. Am. Chem. Soc.*, 2013, **135**, 2013–2036.
- (a) H. Chen, Y. Li, F. Zhang, G. Zhang and X. Fan, *J. Mater. Chem.*, 2011, **21**, 17658–17661; (b) Y.-L. Dong, H.-G. Zhang, Z. U. Rahman, L. Su, X.-J. Chen, J. Hu and X.-G. Chen, *Nanoscale*, 2012, **4**, 3969–3976; (c) J. Xie, H. Cao, H. Jiang, Y. Chen, W. Shi, H. Zheng and Y. Huang, *Anal. Chim. Acta*, 2013, **796**, 92–100; (d) J. Hao, Z. Zhang, W. Yang, B. Lu, X. Ke, B. Zhang and J. Tang, *J. Mater. Chem. A*, 2013, **1**, 4352–4357.
- (a) G. Nie, L. Zhang, X. Lu, X. Bian, W. Sun and C. Wang, *Dalton Trans.*, 2013, **42**, 14006–14013; (b) X. Chen, X. Tian, B. Su, Z. Huang and M. Oyama, *Dalton Trans.*, 2014, **43**, 7449–7454; (c) Y. Ye, T. Kong, X. Yu, Y. Wu, K. Zhang and X. Wang, *Talanta*, 2012, **89**, 417–421; (d) M. I. Kim, M. S. Kim, M.-A. Woo, Y. Ye, K. S. Kang, J. Lee and H. G. Park, *Nanoscale*, 2014, **6**, 1529–1536; (e) Y. Tao, Y. Lin, Z. Huang, J. Ren and X. Qu, *Adv. Mater.*, 2013, **25**, 2594–2599; (f) L.-N. Zhang, H.-H. Deng, F.-L. Lin, X.-W. Xu, S.-H. Weng, A.-L. Liu, X.-H. Lin, X.-H. Xia and W. Chen, *Anal. Chem.*, 2014, **86**, 2711–2718; (g) L. Deng, C. Chen, C. Zhu, S. Dong and H. Lu, *Biosens. Bioelectron.*, 2014, **52**, 324–329; (h) Z. Zhang, J. Hao, W. Yang, B. Lu, X. Ke, B. Zhang and J. Tang, *ACS Appl. Mater. Interfaces*, 2013, **5**, 3809–3815; (i) Z. Xing, J. Tian, A. M. Asiri, A. H. Qusti, A. O. Al-Youbi and X. Sun, *Biosens. Bioelectron.*, 2014, **52**, 452–457.
- (a) C. L. Corkhill and D. J. Vaughan, *Appl. Geochem.*, 2009, **24**, 2342–2361; (b) M. J. Hawkesford and L. J. De Kok, *Plant, Cell Environ.*, 2006, **29**, 382–395; (c) E. Pouokam, J. Steidle and M. Diener, *Biol. Pharm. Bull.*, 2011, **34**, 789–793; (d) P. F. Lito, J. P. S. Aniceto and C. M. Silva, *Water, Air, Soil Pollut.*, 2012, **223**, 6133–6155.
- (a) Q. Li and J. R. Lancaster Jr, *Nitric Oxide Biol. Chem.*, 2013, **35**, 21–34; (b) D. J. Polhemus and D. J. Lefer, *Circ. Res.*, 2014, **114**, 730–737; (c) S. Mani, A. Untereiner, L. Wu and R. Wang, *Antioxid. Redox Signaling*, 2014, **20**, 805–817; (d) G. K. Kolluru, X. Shen, S. C. Bir and C. G. Kevil, *Nitric Oxide Biol. Chem.*, 2013, **35**, 5–20.
- (a) S. K. Pandey, K.-H. Kim and K.-T. Tang, *TrAC, Trends Anal. Chem.*, 2012, **32**, 87–99; (b) P. Nagy, Z. Pálkás, A. Nagy, B. Budai, I. Tóth and A. Vasas, *Biochim. Biophys. Acta, Gen. Subj.*, 2014, **1840**, 876–891; (c) X. Hu and B. Mutus, *Rev. Anal. Chem.*, 2013, **32**, 247–256; (d) V. S. Lin and C. J. Chang, *Curr. Opin. Chem. Biol.*, 2012, **16**, 595–601; (e) H. Peng, W. Chen, S. Burroughs and B. Wang, *Curr. Org. Chem.*, 2013, **17**, 641–653.
- M. Zhou, Z. Diwu, N. Panchuk-Voloshina and R. P. Haugland, *Anal. Biochem.*, 1997, **253**, 162–168.
- (a) W. S. Hummers Jr and R. E. Offeman, *J. Am. Chem. Soc.*, 1958, **80**, 1339; (b) D. C. Marcano, D. V. Kosynkin, J. M. Berlin, A. Sinitskii, Z. Sun, A. Slesarev, L. B. Alemany, W. Lu and J. M. Tour, *ACS Nano*, 2010, **4**, 4806–4814.
- B. Zhao, F. A. Summers and R. P. Mason, *Free Radical Biol. Med.*, 2012, **53**, 1080–1087.
- C.-W. Lien, Y.-T. Tseng, C.-C. Huang and H.-T. Chang, *Anal. Chem.*, 2014, **86**, 2065–2072.
- (a) J. V. Rodrigues and C. M. Gomes, *Free Radical Biol. Med.*, 2010, **49**, 61–66; (b) H. H. Gorris and D. R. Walt, *J. Am. Chem. Soc.*, 2009, **131**, 6277–6282.
- (a) S. Wang, *Dyes Pigm.*, 2008, **76**, 714–720; (b) E. G. Garrido-Ramírez, B. K. G. Theng and M. L. Mora, *Appl. Clay Sci.*, 2010, **47**, 182–192; (c) J. V. Coelho, M. S. Guedes, R. G. Prado, J. Tronto, J. D. Ardisson, M. C. Pereira and L. C. A. Oliveira, *Appl. Catal., B*, 2014, **144**, 792–799; (d) N. A. Zubir, C. Yacou, J. Motuzas, X. Zhang and J. C. Diniz da Costa, *Sci. Rep.*, 2014, **4**, 4594.
- (a) F. Peng, T. Luo, L. Qiu and Y. Yuan, *Mater. Res. Bull.*, 2013, **48**, 2180–2185; (b) K. Zhang, V. Dwivedi, C. Chi and J. Wu, *J. Hazard. Mater.*, 2010, **182**, 162–168; (c) M.-L. Chen, L.-M. Shen, S. Chen, H. Wang, X.-W. Chen and J.-H. Wang, *J. Mater. Chem. B*, 2013, **1**, 2582–2589; (d) G. Huang, C. Zhang, Y. Long, J. Wynn, Y. Liu, W. Wang and J. Gao, *Nanotechnology*, 2013, **24**, 395601; (e) Y. Sun, X. Hu, W. Luo, H. Xu, C. Hu and Y. Huang, *ACS Appl. Mater. Interfaces*, 2013, **5**, 10145–10150.
- (a) W. D. Chemelewski, H.-C. Lee, J.-F. Lin, A. J. Bard and C. B. Mullins, *J. Am. Chem. Soc.*, 2014, **136**, 2843–2850; (b) J. Jung, K. Song, D. R. Bae, S. W. Lee, G. Lee and Y.-M. Kang, *Nanoscale*, 2013, **5**, 11845–11849; (c) Z. Xu,

- M. Zhang, J. Wu, J. Liang, L. Zhou and B. Lů, *Water Sci. Technol.*, 2013, **68**, 2178–2185; (d) M. Mohapatra and S. Anand, *Int. J. Eng. Sci. Technol.*, 2010, **2**, 127–146.
- 19 (a) Y. Liu, G.-Q. Qi, C.-L. Liang, R.-Y. Bao, W. Yang, B.-H. Xie and M.-B. Yang, *J. Mater. Chem. C*, 2014, **2**, 3846–38540; (b) K. H. Lee, B. Lee, S.-J. Hwang, J.-U. Lee, H. Cheong, O.-S. Kwon, K. Shin and N. H. Hur, *Carbon*, 2014, **69**, 327–335; (c) A. T. U. Nugrahenny, J. Kim, S.-K. Kim, D.-H. Peck, S.-H. Yoon and D.-H. Jung, *Carbon Lett.*, 2014, **15**, 38–44; (d) J.-H. Yun, Y. H. Ng, R. J. Wong and R. Amal, *ChemCatChem*, 2013, **5**, 3060–3067.
- 20 (a) X. Tian, S. Sarkar, A. Pekker, M. L. Moser, I. Kalinina, E. Bekyarova, M. E. Itkis and R. C. Haddon, *Carbon*, 2014, **72**, 82–88; (b) F. T. Thema, M. J. Moloto, E. D. Dikio, N. N. Nyangiwe, L. Kotsedi, M. Maaza and M. Khenfouch, *J. Chem.*, 2013, 150536.
- 21 A. K. Datta and V. Rakesh, *Compr. Rev. Food Sci. Food Saf.*, 2013, **12**, 24–39.
- 22 C. Qiang, J. Xu, Z. Zhang, L. Tian, S. Xiao, Y. Liu and P. Xu, *J. Alloys Compd.*, 2010, **506**, 93–97.
- 23 P. Klán, J. Literák and S. Relich, *J. Photochem. Photobiol., A*, 2001, **143**, 49–57.
- 24 (a) P. Liu and Y. Huang, *J. Polym. Res.*, 2014, **21**, 430; (b) G. M. Barbosa, M. M. Mosso, C. Vilani, D. R. G. Larrudé, E. C. Romani and L. F. Fernando Jr, *Microw. Opt. Technol. Lett.*, 2014, **56**, 560–563; (c) J. A. Menéndez, A. Arenillas, B. Fidalgo, Y. Fernández, L. Zubizarreta, E. G. Calvo and J. M. Bermúdez, *Fuel Process. Technol.*, 2010, **91**, 1–8.
- 25 (a) J. Zheng, H. Lv, X. Lin, G. Ji, X. Li and Y. Du, *J. Alloys Compd.*, 2014, **589**, 174–181; (b) X. Zhao, Z. Zhang, L. Wang, K. Xi, Q. Cao, D. Wang, Y. Yang and Y. Du, *Sci. Rep.*, 2013, **3**, 3421; (c) L. Wang, Y. Huang, X. Ding, P. Liu, M. Zong and Y. Wang, *Mater. Sci. Eng., B*, 2013, **178**, 1403–1409; (d) L. Wang, Y. Huang, X. Sun, H. Huang, P. Liu, M. Zong and Y. Wang, *Nanoscale*, 2014, **6**, 3157–3164.
- 26 (a) Y. L. Liu, X. J. Zhao, X. X. Yang and Y. F. Li, *Analyst*, 2013, **138**, 4526–4531; (b) G. Reginald and C. M. Grisham, in *Biochemistry*, Cengage Learning, Belmont, 4th edn, 2010, part 2, ch. 13, pp. 406–407; (c) F. Deyhimi and F. Nami, *Int. J. Chem. Kinet.*, 2012, **44**, 699–704; (d) L. S. Zamorano, N. F. Cuadrado, P. P. Galende, M. G. Roig and V. L. Shnyrov, *J. Biophys. Chem.*, 2012, **3**, 16–28.
- 27 (a) Z. Dai, S. Liu, J. Bao and H. Ju, *Chem.–Eur. J.*, 2009, **15**, 4321–4326; (b) A. K. Dutta, S. K. Maji, D. N. Srivastava, A. Mondal, P. Biswas, P. Paul and B. Adhikary, *ACS Appl. Mater. Interfaces*, 2012, **4**, 1919–1927.
- 28 (a) X. Hou, F. Zeng, F. Du and S. Wu, *Nanotechnology*, 2013, **24**, 335502; (b) A. Hatamie, B. Zargar and A. Jalali, *Talanta*, 2014, **121**, 234–238; (c) A. H. Gore, S. B. Vatre, P. V. Anbhule, S.-H. Han, S. R. Patil and G. B. Kolekar, *Analyst*, 2013, **138**, 1329–1333; (d) Z.-X. Wang, C.-L. Zheng, Q.-L. Li and S.-N. Ding, *Analyst*, 2014, **139**, 1751–1755.
- 29 (a) J. Zhang, X. Xu and X. Yang, *Analyst*, 2012, **137**, 1556–1558; (b) Z.-X. Wang, C.-L. Zheng and S.-N. Ding, *RSC Adv.*, 2014, **4**, 9825–9829; (c) A. Pandya, K. V. Joshi, N. R. Modi and S. K. Menon, *Sens. Actuators, B*, 2012, **168**, 54–61; (d) L.-X. Chen, D.-W. Li, L.-L. Qu, Y.-T. Li and Y.-T. Long, *Anal. Methods*, 2013, **5**, 6579–6582.
- 30 (a) X. Cao, W. Lin and L. He, *Org. Lett.*, 2011, **13**, 4716–4719; (b) L. Zhang, X. Lou, Y. Yu, J. Qin and Z. Li, *Macromolecules*, 2011, **44**, 5186–5193; (c) C. Kar and G. Das, *J. Photochem. Photobiol., A*, 2013, **251**, 128–133; (d) M.-Q. Wang, K. Li, J.-T. Hou, M.-Y. Wu, Z. Huang and X.-Q. Yu, *J. Org. Chem.*, 2012, **77**, 8350–8354.